

See discussions, stats, and author profiles for this publication at: <https://www.researchgate.net/publication/270827101>

Experimental and DFT Studies on the Aggregation Behavior of Imidazolium-Based Surface Active Ionic Liquids With Aromatic Counterions in Aqueous Solution.

ARTICLE *in* LANGMUIR · JANUARY 2015

Impact Factor: 4.46 · DOI: 10.1021/la503884v · Source: PubMed

CITATIONS

4

READS

32

7 AUTHORS, INCLUDING:



[Qiong-Zheng Hu](#)

University of Houston

26 PUBLICATIONS 173 CITATIONS

[SEE PROFILE](#)



[Li Yu](#)

Shandong University

114 PUBLICATIONS 1,966 CITATIONS

[SEE PROFILE](#)

Experimental and DFT Studies on the Aggregation Behavior of Imidazolium-Based Surface-Active Ionic Liquids with Aromatic Counterions in Aqueous Solution

Wenwen Xu,^{†,‡} Tao Wang,[§] Ni Cheng,[†] Qiongzheng Hu,^{||} Yanhui Bi,[†] Yanjun Gong,[†] and Li Yu^{*,†,‡}

[†]Key Laboratory of Colloid and Interface Chemistry, Shandong University, Ministry of Education, Jinan 250100, P. R. China

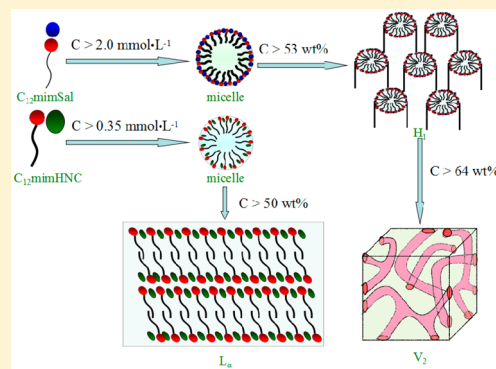
[‡]School of Chemistry and Chemical Engineering, Qufu Normal University, Qufu, 273165, P. R. China

[§]Production Technology Institute, Shengli Oilfield, Dongying, 257000, P. R. China

^{||}Department of Chemistry, University of Houston, Houston, Texas 77204, United States

Supporting Information

ABSTRACT: Two imidazolium-based surface-active ionic liquids with aromatic counterions, namely, 1-dodecyl-3-methylimidazolium salicylate ($C_{12}\text{mimSal}$) and 1-dodecyl-3-methylimidazolium 3-hydroxy-2-naphthoate ($C_{12}\text{mimHNC}$), were synthesized, and their aggregate behavior in aqueous solutions was systematically explored. Surface tension and conductivity measurements indicate that both $C_{12}\text{mimSal}$ and $C_{12}\text{mimHNC}$ show superior surface activity compared to the common imidazolium-based SAIL with the same hydrocarbon chain length, 1-dodecyl-3-methylimidazolium bromide ($C_{12}\text{mimBr}$). This result demonstrates that the incorporation of aromatic counterions favors the formation of micelles. $C_{12}\text{mimHNC}$ displays a higher surface activity than $C_{12}\text{mimSal}$, resulting from the different hydrophobicities of the counterions. In comparison with $C_{12}\text{mimBr}$, $C_{12}\text{mimSal}$ not only can form hexagonal liquid-crystalline phase (H_1) in aqueous solution, but also exhibits a broad region of cubic liquid-crystalline phase (V_2) at higher concentration. As for the $C_{12}\text{mimHNC}/\text{H}_2\text{O}$ system, a lamellar liquid-crystalline (L_a) phase was observed. These lyotropic liquid crystals (LLCs) were characterized by polarized optical microscopy (POM) and small-angle X-ray scattering (SAXS). Structural parameters calculated from SAXS patterns suggest that a higher concentration of the SAIL leads to a denser arrangement whereas a higher temperature results in the opposite effect. The rheological results manifest that the formed H_1 phase in the $C_{12}\text{mimSal}/\text{H}_2\text{O}$ system exhibits an impressive viscoelastic behavior, indicated by a modulus (G' and G'') that is 1 order of magnitude higher than that of $C_{12}\text{mimBr}$. Density functional theory (DFT) calculations reveal that $C_{12}\text{mimSal}$ has a more negative interaction energy with a water molecule and the Sal^- counterion presents a stronger electronegativity than the HNC^- counterion. The specific phase behavior of the $C_{12}\text{mimSal}/\text{H}_2\text{O}$ and $C_{12}\text{mimHNC}/\text{H}_2\text{O}$ systems can be attributed to the strong synergic interaction between the imidazolium cation and the aromatic counterion, including electrostatic attraction, hydrophobic interaction, and especially $\pi-\pi$ interaction.



1. INTRODUCTION

With the rising challenges of environmentally benign chemical processing, ionic liquids (ILs), consisting of a large organic cation and a corresponding small anion, have emerged in recent years.^{1,2} They have been shown to be excellent candidates in the fields of catalysis, nanostructure materials, organic synthesis, electrochemistry, and liquid/liquid extraction.^{3–7} More importantly, their chemical and physical properties can be effectively and easily tailored by changing the cation, anion, and substituent components.⁸ ILs bearing long alkyl chain can be regarded as a novel category of amphiphiles. Owing to their inherent molecular nature, they are called surface-active ionic liquids (SAILS), and they can form aggregates with specific structures, shapes, and properties. The aggregation behavior of SAILS has therefore been extensively investigated in the field of colloid and interface chemistry.

Generally, surfactant molecules can aggregate to form thermodynamically stable self-assembled structures, such as micelles, vesicles, microemulsions, and lyotropic liquid crystals (LLCs).^{9–11} Among them, LLCs, including hexagonal (H_1), cubic (V_2), and lamellar (L_a) liquid-crystalline phases, have become a significant subject because of their wide applications in chemical reactions, materials science, and pharmaceutical vehicles.^{12–15} Recently, LLCs formed from SAILS have attracted increasing attention. Firestone et al.¹⁶ documented the phase behavior of 1-decyl-3-methylimidazolium bromide ($C_{10}\text{mimBr}$) in aqueous solution and found that, at room temperature, it could turn into a stable, homogeneous liquid-

Received: September 30, 2014

Revised: January 9, 2015

Published: January 12, 2015

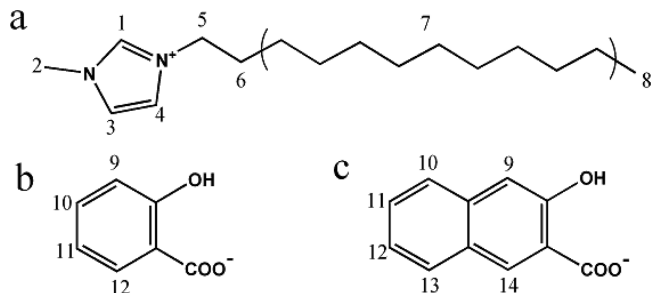


crystalline gel at the composition range of 5–40 wt % H₂O. In addition, Zhao et al. studied LLCs formed by *N*-alkyl-*N*-methylpiperidinium bromides (C_n PDB, $n = 12, 14, 16$), illustrating that different hydrophobic interactions result in different types of phase diagrams in water.¹⁷ LLCs aggregated by *N*-alkyl-*N*-methylpyrrolidinium bromides in water and ethylammonium nitrate (EAN) were also reported, which confirmed that the solvent effect on the phase behavior could not be neglected.¹⁸

However, so far, there have been only a few investigations of the LLCs formed by SAILs containing various counterions. Zheng's group prepared a novel single-tailed SAIL with an aromatic anion, 1-dodecyl-3-methylimidazolium β -naphthalenesulfonate (C_{12} mimNsa), and observed a spontaneous phase transition from the micellar phase to the vesicle phase and then to the lamellar liquid-crystal phase with increasing concentration of C_{12} mimNsa.¹⁹ Biswas et al. investigated the phase behavior of imidazolium-based ionic liquids with different fatty acid anions by polarized optical microscopy (POM), powder X-ray diffraction (PXRD), and differential scanning calorimetry (DSC) and found that an interdigitated bilayer arrangement of the crystalline phase was extended.²⁰ A novel acid soap, prepared from pyrrolidine and fatty acid, was detected to form a lamellar liquid crystal stabilized by hydrogen bonds between two interacting six-membered rings.²¹ We investigated the self-assembly behavior of 1-butyl-3-methylimidazolium dodecylsulfate ($[C_4\text{mim}][C_{12}\text{H}_2\text{SO}_4]$) in water/ethylammonium nitrate (EAN) mixed solvents with different volume ratios and found that the system could form lyotropic liquid crystals with multimesophases, namely, normal hexagonal (H_1), lamellar liquid crystal (L_a), and reverse bicontinuous cubic phase (V_2), in the water-rich environment.²²

Based on previous studies of the aggregation behavior of alkylsulfate^{22–25} and alkylcarboxylate^{26,27} based SAILs, this work aims to investigate the $\pi-\pi$ interaction between the aromatic counterion and the imidazolium headgroup, which might lead to an unexpected effect on their self-assembly behavior compared with that of imidazolium-based ionic liquids containing halogen counterions, which always forms aggregates such as vesicles or wormlike micelles.^{28,29} In the present work, two SAILs with aromatic counterions, namely, 1-dodecyl-3-methylimidazolium salicylate (C_{12} mimSal) and 1-dodecyl-3-methylimidazolium 3-hydroxy-2-naphthoate (C_{12} mimHNC) (chemical structures are shown in Scheme 1), were synthesized. Although the highly luminescent and color-tunable salicylate ionic liquid C_{12} mimSal was reported by Campbell et al.,³⁰ they focused on only its thermal, structural, and photophysical properties. However, the main aim of this work is to investigate

Scheme 1. Chemical Structures of (a) C_{12} mim⁺, (b) Sal⁻, and (c) HNC⁻



the effect of the $\pi-\pi$ interaction between the aromatic counterion and the imidazolium headgroup on the self-assembly behavior (e.g., micelles and lyotropic liquid crystals) of SAILs. This comparative study shows that aromatic counterions play a significant role in the surface activities, aggregate structures, and properties. We expect that the present work can enrich the applications of SAILs in materials preparation, drug delivery, and DNA release, among others.

2. EXPERIMENTAL SECTION

2.1. Materials. 1-Methylimidazole (99%) was obtained from Acros Organics and distilled prior to use. 1-Bromododecane (98%), sodium salicylate (NaSal) (99%), and 3-hydroxy-2-naphthoic acid (98%) were all purchased from J&K Scientific Co., Ltd., and used as received. Dichloromethane, ethyl acetate, ethyl alcohol, and acetone were all obtained from Tianjin Fuyu Chemical Reagent Company of China. Triply distilled water was used to prepare aqueous solutions.

2.2. Synthesis of SAILs. **2.2.1. Synthesis of C_{12} mimSal.** C_{12} mimBr was prepared according to the procedures reported previously.²⁰ C_{12} mimBr and NaSal with a molar ratio of 1:1 were dissolved in a mixed solvent of ethanol and acetone (1:3, v/v). The mixture was stirred at 50 °C for 8 h, and then the insoluble NaBr was filtered off. After evaporation of the solvent, the obtained product was purified by recrystallization in ethyl acetate at least four times. The purity of the final product was tested by AgNO₃. Finally, the product was dried under a vacuum for 48 h.

2.2.2. Synthesis of C_{12} mimHNC. C_{12} mimHNC was synthesized by the neutralization method. An aqueous solution of C_{12} mimBr was allowed to pass through a column that was filled with anion-exchange resin to obtain C_{12} mimOH. Then, the C_{12} mimOH aqueous solution was neutralized with equimolar 3-hydroxy-2-naphthoic acid. C_{12} mimHNC was obtained after removal of the water and was dried under a vacuum for 48 h at 55 °C.

The purities of both C_{12} mimSal and C_{12} mimHNC were ascertained by ¹H NMR spectroscopy on a Bruker Avance 300 spectrometer (details presented in the Supporting Information). The melting points of C_{12} mimSal and C_{12} mimHNC were found to be (47 ± 1) and (60 ± 1) °C, respectively, as determined on an XD-4 digital micro melting point apparatus. Thus, the imidazolium-based surfactants prepared in this work are ILs (with melting points below 100 °C) and can be called SAILs.

2.3. Micellization of C_{12} mimSal and C_{12} mimHNC. Surface tension measurements were carried out on a model JYW-200B tensiometer (Chengde Dahu Instrument Co., Ltd., Chengde, Hebei, China; accuracy of ±0.1 mN/m) using the ring method. Electrical conductivity was performed on a low-frequency conductivity analyzer (model DDSJ-308A, Shanghai Precision & Science Instrument Co., Ltd., Shanghai, China). Each electrical conductivity data point was recorded when its stability was better than 1% within 2 min. The temperature of surface tension and electrical conductivity measurements was controlled by a thermostatic water bath with an uncertainty of within ±0.1 °C.

2.4. Sample Preparation and Phase Diagram Mapping. Samples were prepared by weighing the designed compositions (in weight percentages) of the SAILs and H₂O in stoppered glass vials. The samples were mixed using a vortex mixer and repeated centrifugation. Then, they were stored in a thermostat for at least 2 weeks for equilibration before further investigations. POM and small-angle X-ray scattering (SAXS) were applied to determine the LLC type and establish the corresponding phase diagrams. The composition interval was first selected as 5 wt % for a rough mapping, whereas 2 wt % was chosen for the identification of the phase boundaries.

2.5. Characterization. **2.5.1. Polarized Optical Microscopy Observation.** A Motic B2 polarized optical microscope equipped with a CCD camera (Panasonic Super Dynamic II WV-CP460) was used to take photographs of sample birefringence.

2.5.2. Small-Angle X-ray Scattering Measurements. The structural characterizations of LLCs were performed in an Anton Paar SAXSess mc² system with Ni-filtered Cu K α radiation (0.154 nm) operating at 2

kW (50 kV and 40 mA). The LLC samples were placed in a stainless steel tank and sealed with transparent film. The distance between the sample and the detector was 264.5 mm. All samples were held in a vacuum steel holder to provide thermal contact with the computer-controlled Peltier heating system (Hecus MBraun, Graz, Austria).

2.5.3. Rheological Measurements. The rheological properties were measured on a Haake RS75 rheometer with a cone–plate sensor (Ti, diameter = 35 mm, cone angle = 1°, distance = 52 μm). Frequency sweep measurements were performed at a constant stress, which was determined from the strain sweep measurements.

3. RESULTS AND DISCUSSION

3.1. Micellization of C₁₂mimSal and C₁₂mimHNC Systems. Surface tension and electrical conductivity measurements were carried out to characterize the surface activity and micellization thermodynamic properties of C₁₂mimSal and C₁₂mimHNC.

Figure 1 shows surface tension (γ) versus concentration (C) plots obtained for the investigated SAILs at 25 °C. It is clear

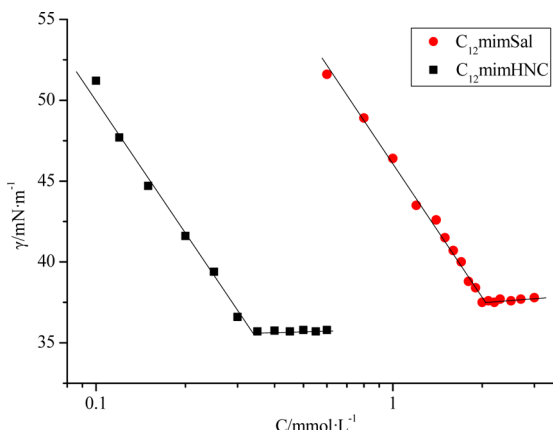


Figure 1. Surface tension plots as a function of concentration for C₁₂mimSal and C₁₂mimHNC in aqueous solution at 25 °C.

that the surface tension decreases gradually with increasing concentration of SAILs, above which a near-plateau region of surface tension appears, suggesting the formation of micelles. The breakpoint in the γ versus C plots is assigned to the critical micelle concentration (cmc), which originates from the micellization of amphiphilic compounds. Note that the absence of a minimum around the breakpoint further confirms the high purity of the two SAILs prepared in this work.

Based on the surface tension plots, the effectiveness of surface tension reduction (Π_{cmc}) and the adsorption efficiency (pC_{20}) of the SAILs at the air/water interface were obtained according to the equation reported earlier.³¹ Applying the Gibbs adsorption isotherm to the surface tension plots,³² the maximum surface excess concentration (Γ_{\max}) and the minimum surface area per molecule at the interface (A_{\min}) were also calculated. The estimated surface property parameters

for C₁₂mimSal and C₁₂mimHNC, together with the previously reported data for C₁₂mimBr,³³ are all listed in Table 1.

As observed in Table 1, the cmc values of C₁₂mimSal, C₁₂mimHNC, and C₁₂mimBr are 2.0, 0.35, and 10.9 mmol·L⁻¹, respectively, which demonstrates that C₁₂mimHNC has the strongest ability to form micelles. It is also obvious that the Π_{cmc} and pC_{20} values of C₁₂mimHNC are both larger than those of C₁₂mimSal and C₁₂mimBr, revealing that C₁₂mimHNC is superior in terms of the effectiveness and efficiency of the surface tension reduction that it provides. It has been reported that both electrostatic interactions and hydrophobic interactions can contribute to the formation of micelles.³⁴ Thus, the differences associated with the properties of these SAILs can be ascribed to the following two reasons: First, the electrostatic repulsion between headgroups is reduced more effectively for the weaker hydration of the aromatic counterion than the inorganic anion, thereby resulting in a variation in cmc values. Second, aromatic counterions enhance the hydrophobic interactions of SAIL molecules and play a crucial role in facilitating micelle formation. Therefore, the cmc values of the investigated SAILs are smaller than that of the traditional imidazolium-based SAIL, C₁₂mimBr. The smaller cmc and γ_{cmc} values of C₁₂mimHNC compared with C₁₂mimSal can be attributed to the introduction of an additional benzene ring, which strengthens the hydrophobicity of the counterion and thus improves its surface activity.

From Table 1, the maximum surface excess concentration, Γ_{\max} , and the area occupied by a single surfactant molecule at the air/liquid interface, A_{\min} , can also be noted. They were estimated according to the Gibbs adsorption isotherm.³⁵ The Γ_{\max} value increases in the order C₁₂mimBr < C₁₂mimHNC < C₁₂mimSal, whereas the A_{\min} value decreases in the same order. The higher Γ_{\max} values and lower A_{\min} values of C₁₂mimSal and C₁₂mimHNC compared with C₁₂mimBr indicate denser arrangements of the investigated SAIL molecules at the air/liquid interface,³⁶ which can be mainly attributed to the $\pi-\pi$ interaction offered by the aromatic counterions. For C₁₂mimSal and C₁₂mimHNC, the larger steric-hindrance effect induced by the additional benzene ring of the latter results in lower Γ_{\max} and higher A_{\min} values.

Figure 2 shows the variation of the electrical conductivity for C₁₂mimSal and C₁₂mimHNC at different temperatures. The experimental results fit into two straight lines with a substantial change of slope. The breakpoint of the curves corresponds to the cmc. The cmc values at different temperatures and the thermodynamic parameters obtained according to the equations shown in the Supporting Information are summarized in Table 2. Obviously, the cmc values of C₁₂mimSal and C₁₂mimHNC at 25 °C obtained by the electrical conductivity method agree well with those obtained from surface tension measurements. It can be observed that their cmc values increase with the temperature. As shown in Table 2, the ΔG_m^θ values for both SAILs are negative in the investigated temperature range, which indicates that their micellization process in aqueous

Table 1. Surface Properties of C₁₂mimSal, C₁₂mimHNC, and C₁₂mimBr in Aqueous Solution at 25 °C

SAIL	cmc (mmol·L ⁻¹)	γ_{cmc} (mN·m ⁻¹)	pC_{20}	Π_{cmc} (mN·m ⁻¹)	Γ_{\max} (μmol·m ⁻²)	A_{\min} (nm ²)
C ₁₂ mimSal	2.00	37.50	3.04	35.10	3.25	0.51
C ₁₂ mimHNC	0.35	35.50	3.66	37.10	2.16	0.77
C ₁₂ mimBr ^a	10.9	39.4	2.6	33.6	1.91	0.87

^aReported in ref 33.

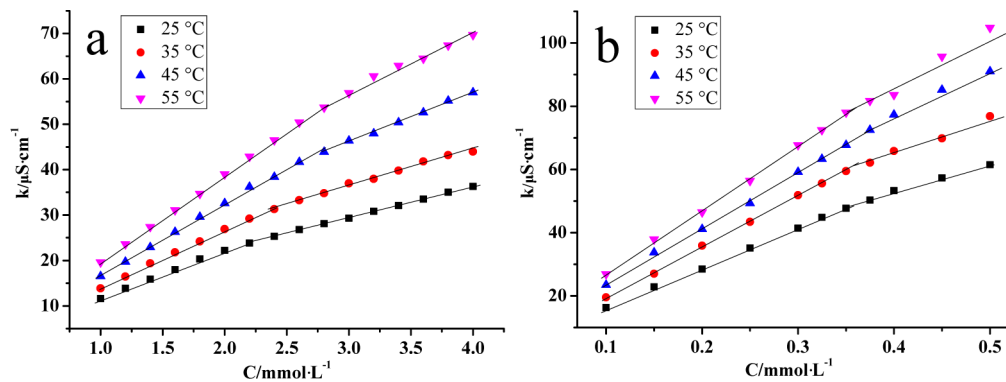


Figure 2. Plots of electrical conductivity as a function of concentration for (a) $C_{12}\text{mimSal}$ and (b) $C_{12}\text{mimHNC}$ in aqueous solution at different temperatures.

Table 2. Critical Micelle Concentration Estimated from Electrical Conductivity Measurements, Degree of Counterion Binding (β), and Thermodynamic Parameters of Micellization for $C_{12}\text{mimSal}$ and $C_{12}\text{mimHNC}$ at Different Temperatures

T (°C)	cmc (mmol·L ⁻¹)	β	ΔG_m^θ (kJ·mol ⁻¹)	ΔH_m^θ (kJ·mol ⁻¹)	$-T\Delta S_m^\theta$ (kJ·mol ⁻¹)
$C_{12}\text{mimSal}$					
25	2.21	0.37	-34.31	-10.00	-24.31
35	2.40	0.39	-35.69	-10.84	-24.85
45	2.62	0.31	-34.59	-10.84	-23.65
55	2.97	0.36	-36.44	-12.04	-24.40
$C_{12}\text{mimHNC}$					
25	0.36	0.32	-39.06	-0.65	-38.41
35	0.36	0.31	-40.07	-0.69	-39.38
45	0.37	0.18	-37.18	-0.66	-36.52
55	0.37	0.15	-37.37	-0.69	-36.68

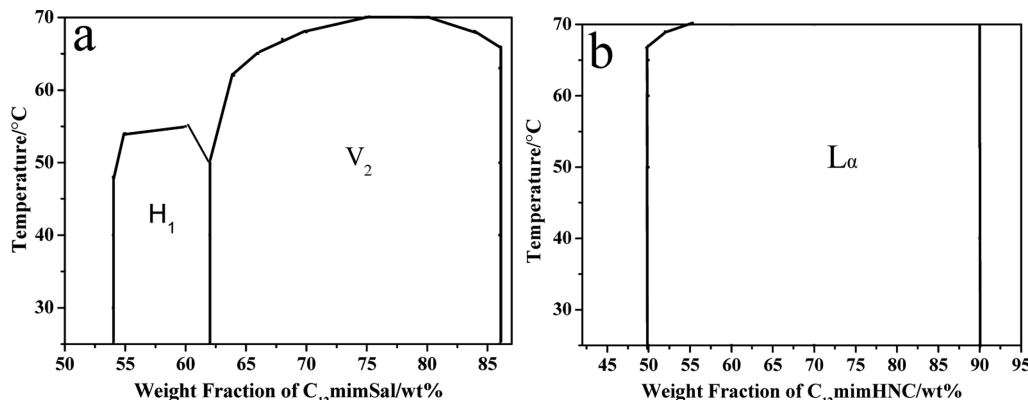


Figure 3. Phase diagrams for the (a) $C_{12}\text{mimSal}/\text{H}_2\text{O}$ and (b) $C_{12}\text{mimHNC}/\text{H}_2\text{O}$ binary mixtures.

solution is spontaneous. The entropic contribution, an effect common in aggregation behaviors driven by hydrophobicity, is a primary element for the negative values of the Gibbs free energy. The data also show that the ΔH_m^θ values of all systems are negative, which implies that the micellization process is exothermic. Compared to $C_{12}\text{mimSal}$, $C_{12}\text{mimHNC}$ has a more negative ΔG_m^θ value, demonstrating that the introduction of a naphthalene ring enhances the hydrophobic interaction between SAIL molecules and facilitates the formation of micelles.

3.2. Phase Diagrams of the $C_{12}\text{mimSal}/\text{H}_2\text{O}$ and $C_{12}\text{mimHNC}/\text{H}_2\text{O}$ Systems. The binary phase diagrams of the $C_{12}\text{mimSal}/\text{H}_2\text{O}$ and $C_{12}\text{mimHNC}/\text{H}_2\text{O}$ systems in the temperature range of 25–70 °C are presented in Figure 3. As shown in Figure 3a, the phase diagram of the $C_{12}\text{mimSal}/\text{H}_2\text{O}$

binary mixture includes three single-phase regions consisting of one isotropic solution phase, one anisotropic hexagonal liquid-crystalline phase (H_1), and one isotropic cubic liquid-crystalline phase (V_2). At 25 °C, a homogeneous and isotropic solution appears, corresponding to the common micellar phase at lower $C_{12}\text{mimSal}$ concentrations (less than 53 wt %). When the concentration of $C_{12}\text{mimSal}$ is greater than 53 wt %, the H_1 phase forms. A further increase in $C_{12}\text{mimSal}$ concentration (64–86 wt %) leads to the appearance of a broad area of V_2 phase. For the $C_{12}\text{mimHNC}/\text{H}_2\text{O}$ mixture, at a relative low SAIL concentration (less than 50 wt %), the mixture is an isotropic, clear, and transparent solution. With increasing $C_{12}\text{mimHNC}$ concentration, the mixture becomes more viscous. Figure 3b shows that lamellar liquid-crystalline phase

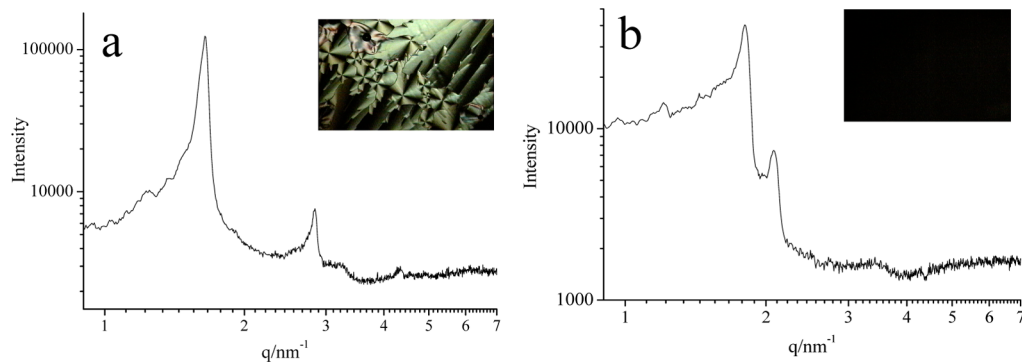


Figure 4. SAXS curves and (insets) POM images for (a) the H₁ phase formed by 50 wt % C₁₂mimSal and (b) the V₂ phase formed by 80 wt % C₁₂mimSal at 25 °C.

(L_α) can be formed in the concentration range of 55–90 wt %, even when the temperature is up to 70 °C.

POM and SAXS were employed to identify H₁ and V₂ phases aggregated successively by C₁₂mimSal and the L_α phase formed by C₁₂mimHNC in aqueous solutions. The SAXS pattern (Figure 4a) of the 55 wt % C₁₂mimSal system shows four distinct peaks with relative *q* values in the ratio of *q*₁/*q*₂/*q*₃/*q*₄ = 1: $\sqrt{3}$:2: $\sqrt{7}$, which is characteristic for hexagonal phases. The observed characteristic “fanlike” textures (Figure 4a, inset) further demonstrate the formation of the H₁ phase. For 80 wt % C₁₂mimSal, two strong scattering peaks in the SAXS spectrum (Figure 4b) were found, with their positions satisfying the relationship $\sqrt{3}:\sqrt{4}$, suggesting the existence of the V₂ phase. The POM image displays only a dark background, indicating an isotropic phase. Moreover, compared with the micellar phase, this mixture cannot flow and is even stiffer than the H₁ phase, suggesting the formation of a cubic phase.¹⁷ In contrast, for the C₁₂mimHNC (70 wt %) system, two Bragg peaks in the SAXS curve (Figure 5) with relative positions of

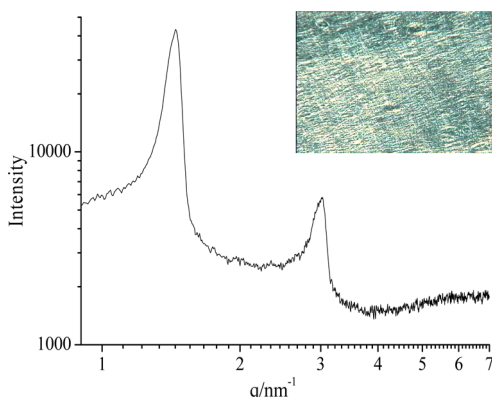


Figure 5. SAXS curve and (inset) POM image of the L_α phase for the 70 wt % C₁₂mimHNC system at 25 °C.

1:2 confirm the existence of the lamellar phase. In addition, the POM image (Figure 5, inset) at 25 °C exhibits oily streaks, which is the representative texture for the L_α phase.

Compared with the liquid-crystalline phase formed by C₁₂mimBr, C₁₂mimSal and C₁₂mimHNC exhibit specific phase behavior at higher concentrations. As reported previously, when the concentration of C₁₂mimBr reaches 44 wt %,³⁷ the C₁₂mimBr/H₂O system can form only the H₁ phase at 25 °C. In contrast, for C₁₂mimSal, the H₁ phase appears until the concentration reaches 53 wt %. Moreover, a large-region V₂

phase is present at 64–86 wt % in the C₁₂mimSal/H₂O system. In addition, analogously to 1-dodecyl-3-methylimidazolium β -naphthalenesulfonate (C₁₂mimNsa),²⁰ the L_α phase is formed at 50 wt % C₁₂mimHNC. These results imply that the π – π interaction between the aromatic anion and imidazolium cation plays a central role in decreasing the minimum surface area per surfactant molecule (*A*_{min}) when the concentration of SAILs with aromatic counterions increases. Moreover, it results in a higher critical packing parameter (*P*), suggesting the emergence of cubic and lamellar phases.

3.3. Effect of SAIL Concentration on Phase Behavior.

From the SAXS patterns (Figure 6a) for the H₁ phase of

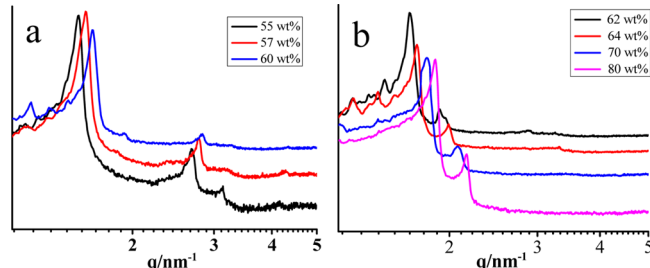


Figure 6. SAXS curves of the (a) H₁ and (b) V₂ phases formed by different concentrations of C₁₂mimSal aqueous solution at 25 °C.

C₁₂mimSal, it is obvious that the first Bragg peak shifts to the right at higher C₁₂mimSal concentrations, implying a smaller distance between the adjacent cylinders. The lattice parameter (*a*₀) was determined to be 41.34, 40.71, and 39.77 Å for 55, 57, and 60 wt % C₁₂mimSal, respectively, which means that the *a*₀ value decreases with increasing C₁₂mimSal concentration. Compared with the parameters of the hexagonal phase formed by the SDS/H₂O system at the same concentration,³⁸ the *a*₀ value for the C₁₂mimSal/H₂O system is smaller. A possible reason for the difference is that the salicylic anion offers a stronger electrostatic screening effect and π – π interaction with the imidazolium headgroup, which decreases the electrostatic repulsion between polar headgroups. Therefore, this causes denser cylindrical aggregates with a smaller *a*₀ value in the C₁₂mimSal/H₂O system.

The H₁ phase consists of infinitely long cylinderlike aggregates packed in a hexagonal array and separated by a continuous solvent region,³⁹ where the hydrophobic tails are located in the interior part of the cylinderlike aggregates and the hydrophilic headgroups are solvated by H₂O molecules.¹⁸ A series of structural parameters, including *a*₀, the radius of a

cylindrical aggregate (d_H), the thickness of the solvent layer (d_W) between cylinders, and the area per molecule at the hydrophilic/hydrophobic interface (a_S), were calculated according to the equations provided in the Supporting Information. The evaluated data are summarized in Table 3.

Table 3. Structural Parameters for the Lypotropic Liquid-Crystalline Phases Aggregated by SAILs in Aqueous Solution with Different Concentrations at 25 °C

sample (wt %)	$C_{12}\text{mimSal H}_1$			
	a_0 (Å)	d_H (Å)	d_W (Å)	a_S (Å 2)
55	41.34	16.10	9.14	43.50
57	40.71	16.13	8.45	43.42
60	39.77	16.17	7.43	43.30
sample (wt %)	$C_{12}\text{mimHNC L}_\alpha$			
	a_0 (Å)	d_L (Å)	d_W (Å)	a_S (Å 2)
60	44.56	26.74	17.82	26.19
65	43.33	28.16	15.17	24.87
70	41.34	28.94	12.40	24.20
80	37.18	29.74	7.44	23.55

As shown in Table 3, with increasing concentration of $C_{12}\text{mimSal}$, both the a_0 and d_W values decrease, whereas d_H increases. Similar phenomena have been noted for the N -hexadecyl- N -methylpyrrolidinium bromide ($C_{16}\text{MPB}$)/ H_2O ¹⁸ and N -dodecyl- N -methylpiperidinium bromide ($C_{12}\text{PDB}$)/ H_2O binary systems,¹⁷ as well as the $C_{12}\text{mimBr}/1\text{-butyl-3-methylimidazolium tetrafluoroborate (bmimBF}_4\text{)}/H_2O$ ternary system.⁴⁰ This suggests that the radius of the cylindrical micelles becomes larger and the solvent layer tends to be thinner. In other words, a higher concentration of $C_{12}\text{mimSal}$ in the H_1 phase results in a denser arrangement of $C_{12}\text{mimSal}$ molecules in a hexagonal array. Meanwhile, the area per $C_{12}\text{mimSal}$ molecule decreases from 43.50 to 43.30 Å 2 as the $C_{12}\text{mimSal}$ concentration increases from 55 to 60 wt %, which also reflects the denser arrangement of SAIL molecules inside the cylinders. When compared with the a_S value (44.46 Å 2) of the hexagonal phase aggregated by $C_{12}\text{PDB}$ at a composition of 55 wt %,¹⁷ it is obvious that the $C_{12}\text{mimSal}$ molecule has a smaller area. The strong electrostatic screening effect and π-π interaction offered by the salicylic anion might be responsible for this. The SAXS patterns of the V_2 phase (Figure 6b) formed by the $C_{12}\text{mimSal}/H_2O$ system displays a trend similar to those of the H_1 phase. That is, the first peak position also moves toward a higher q value with increasing content of $C_{12}\text{mimSal}$.

Figure 7 shows the SAXS patterns of representative samples of the L_α phase formed in the $C_{12}\text{mimHNC}/H_2O$ system at 25 °C. It can be seen that, as the $C_{12}\text{mimHNC}$ concentration in the lamellar phase increases, the Bragg peaks shift to the right. The related parameters calculated from the SAXS results are also presented in Table 3. With increasing concentration of $C_{12}\text{mimHNC}$, both a_0 and d_W decrease, whereas d_L increases, meaning that the water channel is compressed by the expanding SAIL bilayer. This phenomenon coincides with the previous study of LLCs formed by other SAILs, such as 1-dodecyl-3-methylimidazolium β-naphthalenesulfonate ([$C_{12}\text{mim}$]-[Nsa])²⁰ and didecylpyrrolidinium bromide (DC₁₀PB).⁴¹ POM was also applied to study the effect of the $C_{12}\text{mimHNC}$ concentration on the L_α phase. As displayed in Figure 8, when the concentration of $C_{12}\text{mimHNC}$ increases in the L_α phase,

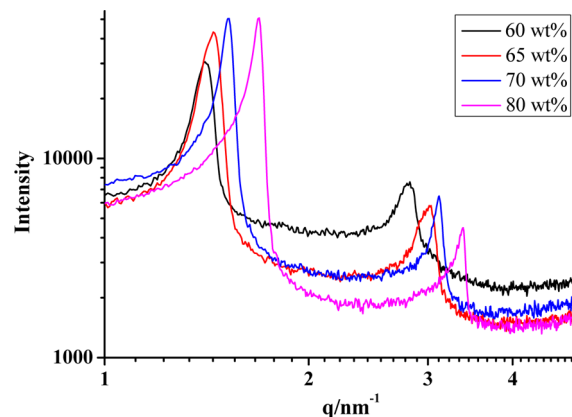


Figure 7. SAXS curves of the L_α phase formed by different concentrations of $C_{12}\text{mimHNC}$ in aqueous solution at 25 °C.

the oily streaks texture formed by the $C_{12}\text{mimHNC}/H_2O$ system becomes denser.

3.4. Effect of Temperature on Phase Behavior. The effect of temperature on the LLCs was investigated by SAXS and POM. From the SAXS patterns in Figure S1a (Supporting Information) for 55 wt % $C_{12}\text{mimSal}$ (representative of the H_1 phase), the Bragg peaks at higher temperature shift to a larger q value, corresponding to a smaller distance between adjacent cylinders. The structural parameters (d_H , d_W , and a_S) calculated from the SAXS patterns are reported in Table 4, from which the variation tendency with temperature can be clearly observed.

With increasing temperature, both d_H and d_W display a declining trend, similarly to $C_{12}\text{PDB}$.¹⁷ This behavior can be attributed to the hydrophobic chains of $C_{12}\text{mimSal}$ molecules becoming soft and extruding each other more with increasing temperature, which leads to a decrease in the cylinder diameter. In addition, a higher temperature weakens the hydrogen-bond interactions among water molecules, which promotes a decrease in d_W . For the V_2 phase, a similar trend is observed. The first peak position of 80 wt % $C_{12}\text{mimSal}$ also shifts to a larger scattering factor at higher temperature (Figure S1b, Supporting Information), in agreement with the trend of the H_1 phase. Figure 9 shows the POM images of the H_1 phase in the $C_{12}\text{mimSal}/H_2O$ system at different temperatures. The fanlike textures still exist even when the temperature is as high as 54 °C.

Figure S2 (Supporting Information) shows the SAXS curves of the L_α phase formed in the $C_{12}\text{mimHNC}/H_2O$ system, which was still stable when the temperature reached 70 °C. Considering the volatility of water, we did not perform further investigations above this temperature. Within the temperature range of 25–70 °C, the Bragg scattering peaks move toward higher q value with increasing temperature, which is analogous to the trends of the H_1 and V_2 phases in the $C_{12}\text{mimSal}/H_2O$ system. Structural parameters deduced from the SAXS curves at different temperatures are included in Table 4. With increasing temperature, d_L and d_W decrease from 26.74 and 17.82 Å to 21.42 and 14.82 Å, respectively. The higher temperature induces the hydrophobic chains of $C_{12}\text{mimHNC}$ to soften and interdigitate more vigorously, so that a decrease in the interlamellar distance occurs.

3.5. Rheological Measurements. The rheological properties were also determined to further investigate the properties of LLCs. For the $C_{12}\text{mimSal}/H_2O$ mixture, the frequency

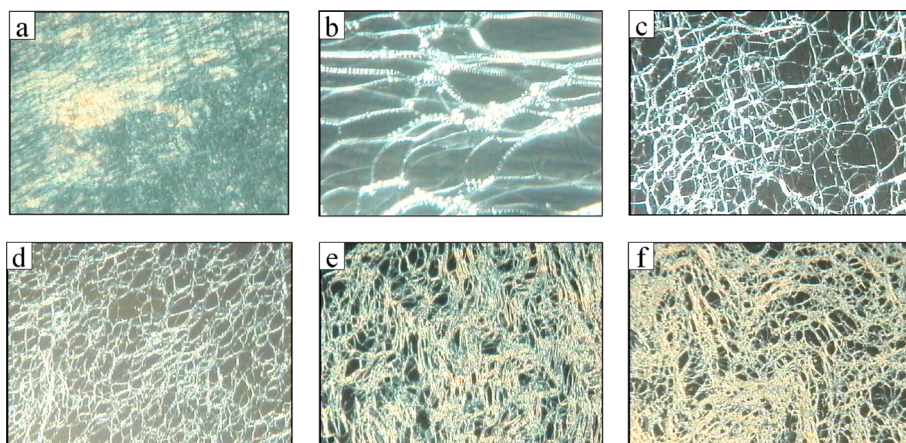


Figure 8. POM images of $C_{12}\text{mimHNC}/\text{H}_2\text{O}$ system with different concentrations of $C_{12}\text{mimHNC}$ at 25°C : (a) 50, (b) 60, (c) 65, (d) 70, (e) 80, and (f) 90 wt %.⁴¹

Table 4. Structural Parameters for the Lypotropic Liquid-Crystalline Phases Aggregated by a Constant Concentration of SAILS in Water at Different Temperatures

$C_{12}\text{mimSal H}_1$ (55 wt %)				
temperature ($^\circ\text{C}$)	a_0 (\AA)	d_H (\AA)	d_W (\AA)	a_S (\AA^2)
25	41.34	16.10	9.14	43.50
40	38.08	14.83	8.42	47.22
50	37.62	14.64	8.34	47.84
$C_{12}\text{mimHNC L}_\alpha$ (60 wt %)				
temperature ($^\circ\text{C}$)	a_0 (\AA)	d_L (\AA)	d_W (\AA)	a_S (\AA^2)
25	44.56	26.74	17.82	26.19
40	41.61	24.97	16.64	28.05
50	39.77	23.86	15.91	29.35
60	38.31	22.99	15.32	30.46
70	35.70	21.42	14.28	32.70

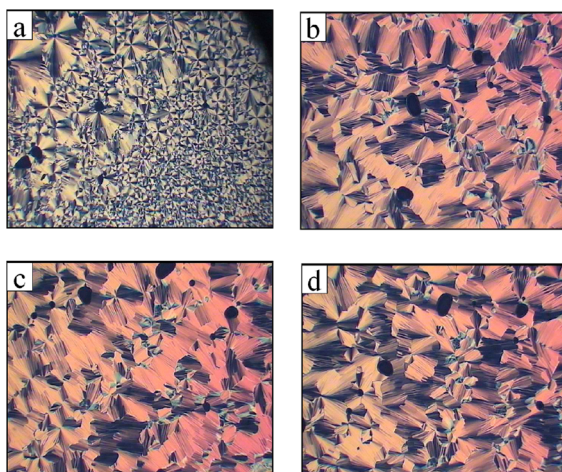


Figure 9. POM images of 55 wt % $C_{12}\text{mimSal}$ in aqueous solution at different temperatures: (a) 25, (b) 47, (c) 51, and (d) 54 $^\circ\text{C}$.⁴²

dependences of the storage modulus (G') and loss modulus (G'') for the H_1 phase are shown in Figure 10a. These results are typical for hexagonal liquid crystals and show traits of a general Maxwell model.⁴² With increasing frequency, the G'' value increases with different slopes at first and then remains nearly constant. The storage modulus (G') is about an order of magnitude higher than the loss modulus (G''). At lower

frequencies, $G'' > G'$, and the system exhibits a viscous behavior. However, at higher frequencies, $G' > G''$, so that the elastic response predominates. This observation demonstrates that the H_1 phase aggregated by $C_{12}\text{mimSal}/\text{H}_2\text{O}$ displays impressive viscoelastic behavior, as the values of G' and G'' are similar to those of the common SAILS N -alkyl- N -methylpiperidinium bromide ($C_n\text{PDB}$)¹⁷ and N -alkyl- N -methylpyrrolidinium bromide ($C_n\text{MPB}$).⁴³

Figure 10b shows the dynamic viscoelastic behavior of the L_α phase formed by the $C_{12}\text{mimHNC}/\text{H}_2\text{O}$ system. The values of G' and G'' remain stable in the investigated frequency region and are almost frequency-independent. G' is about 1 order of magnitude higher than G'' over the whole frequency range studied, which is consistent with the lamellar structures aggregated by other SAILS, such as N -alkyl- N -alkyl'- N,N -dimethylammonium bromide ($C_x\text{C}_y\text{DMABr}$)⁴⁴ and $[C_{12}\text{mim}]\text{-}[Nsa]$.²⁰ Clearly, in comparison with those of lamellar liquid crystals, the rheological parameters of hexagonal liquid crystals increase by 3 orders of magnitude, demonstrating their impressive viscoelastic behavior.

3.6. DFT Calculations. To better understand the interaction between $C_{12}\text{mim}^+$ and the aromatic counterion, we applied density functional theory (DFT) calculations using the Gaussian 09 package with the hybrid B3LYP functional and the 6-31G(d,p) basis.⁴⁵ Figure 11 illustrates the optimized structural models for $C_{12}\text{mimSal}$ and $C_{12}\text{mimHNC}$, in which HNC^- counterion penetrates into the hydrophobic region of $C_{12}\text{mim}^+$ integrally whereas the Sal^- counterion partially binds to the imidazolium headgroup. The alkyl chain length calculated from DFT (Figure 11) is 15 \AA , which is approximately equal to the theoretical value (16.68 \AA) obtained according to the Tanford equation⁴⁶

$$L = 1.5 + 1.265n \quad (1)$$

where n is the number of carbon atoms in the hydrocarbon chain. For the $C_{12}\text{mimSal}$ system, d_H in a hexagonal array is about 16 \AA (Table 3), which means that the hydrophobic alkyl chain stretches in the entire hexagonal phase. In contrast, for $C_{12}\text{mimHNC}$, the d_L value obtained from SAXS measurements is about 28 \AA , which is larger than the alkyl chain length of $C_{12}\text{mimHNC}$ but less than twice its value, indicating a slightly interdigitated bilayer structure.

The interaction energies (E_{int}) for the $C_{12}\text{mimSal}/\text{H}_2\text{O}$ and $C_{12}\text{mimHNC}/\text{H}_2\text{O}$ systems were calculated by the DFT

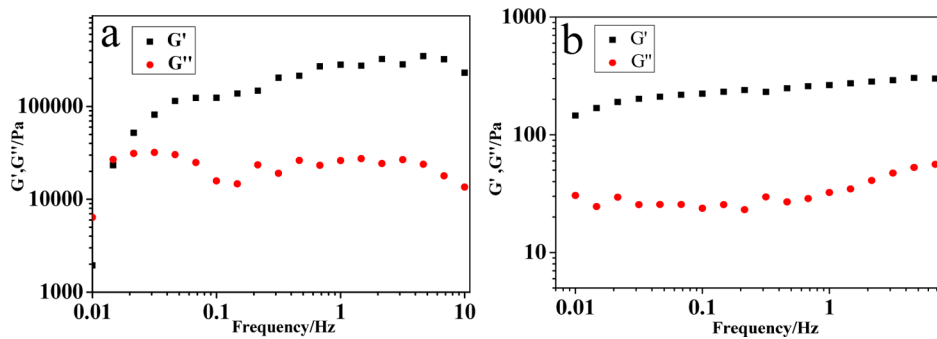


Figure 10. Frequency sweep lines for (a) the H₁ phase of 55 wt % C₁₂mimSal and (b) the L_α phase of 60 wt % C₁₂mimHNC.

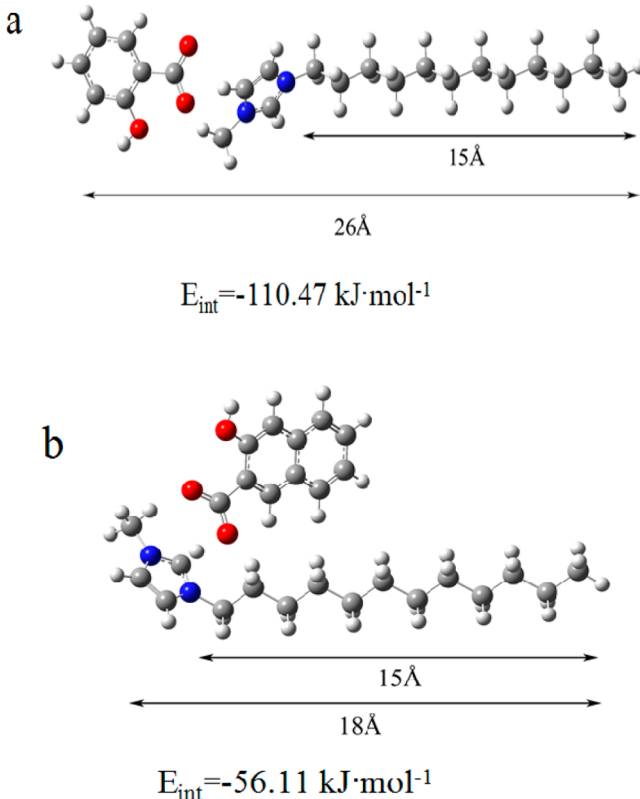


Figure 11. Geometries of (a) C₁₂mimSal and (b) C₁₂mimHNC optimized using the polarizable continuum model at the B3LYP/6-31G(d,p) level.

method to be -110.47 and -56.11 kJ·mol⁻¹, respectively. The more negative interaction energy between the C₁₂mimSal and

H₂O molecules implies a higher stability for the C₁₂mimSal/H₂O complex. This phenomenon means that it is more difficult to destroy the C₁₂mimSal/H₂O complex, which is unfavorable for forming micelles. In other words, for C₁₂mimSal, a stronger interaction with solvent molecules results in a higher cmc value, compared to C₁₂mimHNC.^{47–49} This is consistent with the experimental results (Tables 1 and 2).

For the two SAILs studied in this work, the hydrophilic headgroups are identical, but the counterions are different. Figure 12 depicts the electrostatic potentials at the 0.001 e/bohr³ isodensity surfaces of the Sal⁻ and HNC⁻ counterions. It is obvious that both counterions are electronegative. The less electronegative HNC⁻ counterion means that the electrostatic attraction between HNC⁻ and C₁₂mim⁺ is weaker than that of Sal⁻ and C₁₂mim⁺. This difference, combined with the greater steric hindrance effect caused by the larger size of the HNC⁻ counterion, can primarily account for the lower β value of C₁₂mimHNC (Table 2). Therefore, the electrostatic repulsion between C₁₂mim⁺ ions is screened less effectively by HNC⁻ counterions, which is unfavorable for the formation of micelles by C₁₂mimHNC. However, for C₁₂mimHNC, the stronger hydrophobicity of the HNC⁻ counterion makes it easier to form micelles. The lower cmc value of C₁₂mimHNC (Tables 1 and 2) indicates the dominant role played by the latter factor.

3.7. Mechanisms of the Formation of the LLC Phase.

The critical packing parameter (P) is a classical value used to explain, rationalize, and even predict the self-assembled structure of a particular amphiphile.^{50,51} It is defined as $P = V/AL$, where V is the volume of the hydrophobic chains of the surfactant molecules; A is the effective headgroup area of the surfactant molecules, which is generally obtained by the variation of the surface tension as a function of concentration; and L is the alkyl chain length of the surfactant molecules. In general, the values of P are in the following ranges: for spherical

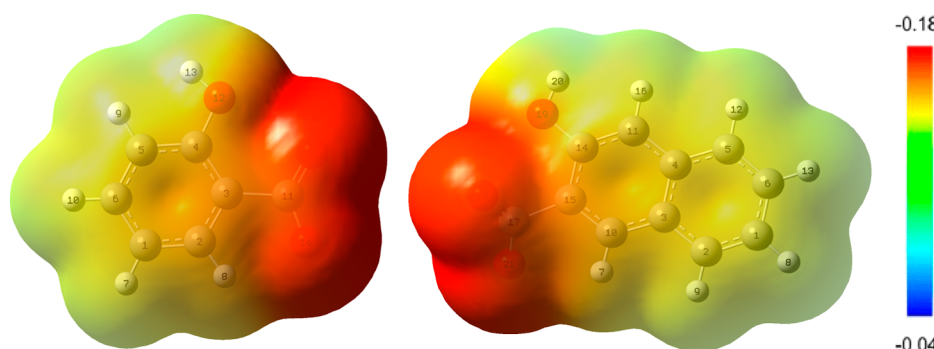


Figure 12. B3LYP/6-31G(d,p) electrostatic potentials, in Hartrees, at 0.001 e/bohr³ isodensity surfaces of the Sal⁻ and HNC⁻ counterions.

micelles, $P \leq 1/3$; for cylindrical aggregates, $1/3 < P \leq 1/2$; for bilayers, vesicles, and bicontinuous cubic LLC phases, $1/2 < P \leq 1$; and for inverted structures, $P > 1$. For the C₁₂mimSal and C₁₂mimHNC molecules, the volume of the hydrophobic chains V can be obtained from the Tanford equation⁴⁶

$$V = 27.4 + 26.9n \quad (2)$$

Then, the V value of the SAILs investigated in this work was calculated to be 350.2 Å³. The hydrocarbon chain length L obtained from DFT calculation is 15 Å. The A_{min} values for C₁₂mimSal and C₁₂mimHNC detected from surface tension measurements are about 51.12 and 76.90 Å², respectively (Table 1). Based on these parameters, the corresponding P values are 0.46 and 0.30, respectively. Therefore, we can speculate that C₁₂mimSal exhibits a strong inclination to pack in a hexagonal array whereas C₁₂mimHNC prefers to form spherical micelles. However, compared to the Sal⁻ counterion, the HNC⁻ counterion binds to the imidazolium cation more strongly with increasing SAIL concentration, because of the cooperative effect of electrostatic, hydrophobic, and π-π interactions.²⁰ Because the electrostatic repulsions between imidazolium headgroups are effectively screened, the P value increases significantly, inducing a phase transition from the micellar phase to the lamellar liquid-crystalline phase.

Compared to the traditional mixtures of common imidazolium-based SAILs and corresponding organic salts that always form aggregates such as wormlike micelles and vesicles,^{52–55} the two “true” salt-free SAIL systems investigated in this work exhibit entirely distinct aggregation behaviors. The excess salt formed in traditional SAIL systems screens the charges of columns or bilayers and decreases the curvature of the micellar or vesicle interface, whereas the high osmotic pressure induced by unscreened electrostatic repulsion in the salt-free SAIL solutions results in the creation of stable aggregates with different morphologies.⁵⁶

4. CONCLUSIONS

In summary, the phase behaviors of novel SAILs with aromatic counterions, namely, C₁₂mimSal and C₁₂mimHNC, were investigated by various techniques, including POM, SAXS, and rheology measurements. In comparison with the common imidazolium-based SAIL C₁₂mimBr, the C₁₂mimSal/H₂O system also formed a large region of cubic liquid-crystalline phase, as well as a hexagonal liquid-crystalline phase. Furthermore, a lamellar liquid-crystalline phase formed in higher-concentration C₁₂mimHNC aqueous solutions. The SAXS results confirm that higher SAIL concentrations in both systems can result in denser aggregation, whereas higher temperatures result in the opposite trend. Rheology measurements indicate that the H₁ phase aggregated by C₁₂mimSal exhibits more outstanding viscoelastic behavior than other common SAILs. In addition, compared to the liquid-crystal systems formed by other common SAILs, the rich and peculiar phase behaviors of the SAILs investigated arise not only from electrostatic interactions between oppositely charged ionic groups and hydrophobic interactions between the alkyl chain of imidazolium cation and apolar portion of counterion, but also from π-π interactions between aromatic counterions. The differences between these two systems are attributed to the presence of diverse counterions. DFT calculations indicate that the more negative interaction energy between C₁₂mimSal and water molecules accounts for its larger cmc and the stronger electronegativity of Sal⁻ accounts for its larger β value. This

work will enrich the investigations of phase behaviors formed in SAIL systems and have potential applications in the fields of nanostructured material fabrication, drug delivery, and so on.

■ ASSOCIATED CONTENT

S Supporting Information

More details about ¹H NMR spectroscopy, theory for the calculation of thermodynamic parameters of micellization, structural parameters of liquid-crystalline phases, and SAXS curves of samples at different temperature. This material is available free of charge via the Internet at <http://pubs.acs.org>.

■ AUTHOR INFORMATION

Corresponding Author

*Phone: +86-531-88364807. Fax: +86-531-88564750. E-mail: ylm1t@sdu.edu.cn.

Notes

The authors declare no competing financial interest.

■ ACKNOWLEDGMENTS

This work was supported by the National Natural Science Foundation of China (No. 21373128), the Scientific and Technological Projects of Shandong Province of China (No. 2014GSF117001), the Natural Science Foundation of Shandong Province of China (No. ZR2011BM017), and the Project of Sinopec (No. P13045).

■ REFERENCES

- (1) Rogers, R. D.; Seddon, K. R. Ionic liquids—Solvents of the future? *Science* **2003**, *302*, 792–793.
- (2) Welton, T. Room-temperature ionic liquids—Solvents for synthesis and catalysis. *Chem. Rev.* **1999**, *99*, 2071–2083.
- (3) Ranu, B. C.; Banerjee, S. Ionic liquid as catalyst and reaction medium. The dramatic influence of a task-specific ionic liquid, [bmim]OH, in Michael addition of active methylene compounds to conjugated ketones, carboxylic esters, and nitriles. *Org. Lett.* **2005**, *7*, 3049–3052.
- (4) Cooper, E. R.; Andrews, C. D.; Wheatley, P. S.; Webb, P. B.; Wormald, P.; Morris, R. E. Ionic liquids and eutectic mixtures as solvent and template in synthesis of zeolite analogues. *Nature* **2004**, *430*, 1012–1016.
- (5) Kuang, D. B.; Brezesinski, T.; Smarsly, B. Hierarchical porous silica materials with a trimodal pore system using surfactant templates. *J. Am. Chem. Soc.* **2004**, *126*, 10534–10535.
- (6) Endres, F.; Bukowski, M.; Hempelmann, R.; Natter, H. Electrodeposition of nanocrystalline metals and alloys from ionic liquids. *Angew. Chem., Int. Ed.* **2003**, *42*, 3428–3430.
- (7) Huddleston, J. G.; Willauer, H. D.; Swatloski, R. P.; Visser, A. E.; Rogers, R. D. Room temperature ionic liquids as novel media for “clean” liquid–liquid extraction. *Chem. Commun.* **1998**, 1765–1766.
- (8) Anouti, M.; Jones, J.; Boisset, A.; Jacquemin, J.; Caravanier, M.C.; Lemordant, D. Aggregation behavior in water of new imidazolium and pyrrolidinium alkylcarboxylates protic ionic liquids. *J. Colloid Interface Sci.* **2009**, *340*, 104–111.
- (9) Abe, M.; Uchiyama, H.; Yamaguchi, T.; Suzuki, T.; Ogin, K. Micelle formation by pure nonionic surfactants and their mixtures. *Langmuir* **1992**, *8*, 2147–2151.
- (10) Schulman, J. H.; Stoeckenius, W.; Princ, L. M. Mechanism of formation and structure of micro emulsions by electron microscopy. *J. Phys. Chem.* **1959**, *63*, 1677–1680.
- (11) Park, J. W.; Bak, C. S.; Labes, M. M. Effects of molecular complexing on the properties of binary nematic liquid crystal mixtures. *J. Am. Chem. Soc.* **1975**, *97*, 4398–4400.
- (12) Taubert, A. CuCl nanoplatelets from an ionic liquid-crystal precursor. *Angew. Chem., Int. Ed.* **2004**, *43*, 5380–5382.

- (13) Gin, D. L.; Gu, W. Q.; Pindzola, B. A.; Zhou, W. J. Polymerized lyotropic liquid crystal assemblies for materials applications. *Acc. Chem. Res.* **2001**, *34*, 973–980.
- (14) Torres, W.; Fox, M. A. Electrosynthesis of polypyrrole in a nematic liquid crystal. *Chem. Mater.* **1992**, *4*, 583–588.
- (15) Nesseem, D. I. Formulation and evaluation of itraconazole via liquid crystal for topical delivery system. *J. Pharm. Biomed. Anal.* **2001**, *26*, 387–399.
- (16) Firestone, M. A.; Dzielawa, J. A.; Zapol, P.; Curtiss, L.A.; Seifert, S.; Dietz, M. L. Lyotropic liquid-crystalline gel formation in a room-temperature ionic liquid. *Langmuir* **2002**, *18*, 7258–7260.
- (17) Zhao, Y. R.; Yue, X.; Wang, X. D.; Chen, X. Lyotropic liquid crystalline phases with a series of *N*-alkyl-*N*-methylpiperidinium bromides and water. *J. Colloid Interface Sci.* **2013**, *389*, 199–205.
- (18) Zhao, M. W.; Gao, Y. A.; Zheng, L. Q. Liquid crystalline phases of the amphiphilic ionic liquid *N*-hexadecyl-*N*-methylpyrrolidinium bromide formed in the ionic liquid ethylammonium nitrate and in water. *J. Phys. Chem. B* **2010**, *114*, 11382–11389.
- (19) Shi, L. J.; Wei, Y.; Sun, N.; Zheng, L. Q. First observation of rich lamellar structures formed by a single-tailed amphiphilic ionic liquid in aqueous solutions. *Chem. Commun.* **2013**, *49*, 11388–11390.
- (20) Biswas, M.; Dule, M.; Samanta, P. N.; Ghosh, S.; Mandal, T. K. Imidazolium-based ionic liquids with different fatty acid anions: Phase behavior, electronic structure and ionic conductivity investigation. *Phys. Chem. Chem. Phys.* **2014**, *16*, 16255–16263.
- (21) Huang, D. D.; Chen, X.; Li, Z. H. Formation of pyrrolidinium fatty acid soap and its lyotropic liquid crystalline phase behavior. *Colloids Surf. A* **2013**, *426*, 55–62.
- (22) Cheng, N.; Hu, Q. Z.; Bi, Y. H.; Xu, W. W.; Gong, Y. J.; Yu, L. Gels and lyotropic liquid crystals: Using an imidazolium-based catanionic surfactant in binary solvents. *Langmuir* **2014**, *30*, 9076–9084.
- (23) Jiao, J. J.; Dong, B.; Zhang, H. N.; Zhao, Y. Y.; Wang, X. Q.; Wang, R.; Yu, L. Aggregation behaviors of dodecyl sulfate-based anionic surface active ionic liquids in water. *J. Phys. Chem. B* **2012**, *116*, 958–965.
- (24) Jiao, J. J.; Han, B.; Liu, M. J.; Cheng, N.; Yu, L.; Liu, M. Salt-free catanionic surface active ionic liquids 1-alkyl-3-methylimidazolium alkylsulfate: Aggregation behavior in aqueous solution. *J. Colloid Interface Sci.* **2013**, *412*, 24–30.
- (25) Jiao, J. J.; Zhang, Y. F.; Fang, L. Y.; Yu, L.; Sun, L. M.; Wang, R.; Cheng, N. Electrolyte effect on the aggregation behavior of 1-butyl-3-methylimidazolium dodecylsulfate in aqueous solution. *J. Colloid Interface Sci.* **2013**, *402*, 139–145.
- (26) Cheng, N.; Yu, P. M.; Wang, T.; Sheng, X.; Bi, Y. H.; Gong, Y. J.; Yu, L. Self-aggregation of new alkylcarboxylate-based anionic surface active ionic liquids: Experimental and theoretical investigations. *J. Phys. Chem. B* **2014**, *118*, 2758–2768.
- (27) Wang, X. Q.; Liu, J.; Yu, L.; Jiao, J. J.; Wang, R.; Sun, L. M. Surface adsorption and micelle formation of imidazolium-based zwitterionic surface active ionic liquids in aqueous solution. *J. Colloid Interface Sci.* **2013**, *391*, 103–110.
- (28) Ye, X. C.; Jin, L. H.; Caglayan, H.; Chen, J.; Xing, G. Z.; Zheng, C.; Doan-Nguyen, V.; Kang, Y. J.; Engheta, N.; Kagan, C. R.; Murray, C. B. Improved size-tunable synthesis of monodisperse gold nanorods through the use of aromatic additives. *ACS Nano* **2012**, *6*, 2804–2817.
- (29) Yu, D. F.; Huang, X.; Deng, M. L.; Lin, Y. Y.; Jiang, L. X.; Huang, J. B.; Wang, Y. L. Effects of inorganic and organic salts on aggregation behavior of cationic gemini surfactants. *J. Phys. Chem. B* **2010**, *114*, 14955–14964.
- (30) Campbell, P. S.; Yang, M.; Pitz, D.; Cybinska, J.; Mudring, A. V. Highly luminescent and color-tunable salicylate ionic liquids. *Chem.—Eur. J.* **2014**, *20*, 4704–4712.
- (31) Rosen, M. J. *Surfactants and Interfacial Phenomena*, 2nd ed.; Wiley: New York, 1989.
- (32) Jaycock, M. J.; Parfitt, G. D. *Chemistry of Interfaces*; John Wiley & Sons: New York, 1981.
- (33) Dong, B.; Li, N.; Zheng, L. Q.; Yu, L.; Inoue, T. Surface adsorption and micelle formation of surface active ionic liquids in aqueous solution. *Langmuir* **2007**, *23*, 4178–4182.
- (34) Dong, B.; Zhao, X. Y.; Zheng, L. Q.; Zhang, J.; Li, N.; Inoue, T. Aggregation behavior of long-chain imidazolium ionic liquids in aqueous solution: Micellization and characterization of micelle microenvironment. *Colloids Surf. A* **2008**, *317*, 666–672.
- (35) Anouti, M.; Jones, J.; Boisset, A.; Jacquemin, J.; Magaly, C. C.; Lemordant, D. Aggregation behavior in water of new imidazolium and pyrrolidinium alkylcarboxylates protic ionic liquids. *J. Colloid Interface Sci.* **2009**, *340*, 104–111.
- (36) Miki, K.; Westh, P.; Nishikawa, K.; Koga, Y. Effect of an “ionic liquid” cation, 1-butyl-3-methylimidazolium, on the molecular organization of H_2O . *J. Phys. Chem. B* **2005**, *109*, 9014–9019.
- (37) Inoue, T.; Dong, B.; Zheng, L. Q. Phase behavior of binary mixture of 1-dodecyl-3-methylimidazolium bromide and water revealed by differential scanning calorimetry and polarized optical microscopy. *J. Colloid Interface Sci.* **2007**, *307*, 578–581.
- (38) Leigh, I. D.; McDonald, M. P.; Wood, R. M.; Tiddy, G. J. T.; Trevethan, M. A. Structure of liquid-crystalline phases formed by sodium dodecyl sulphate and water as determined by optical microscopy, X-ray diffraction and nuclear magnetic resonance spectroscopy. *J. Chem. Soc., Faraday Trans. 1* **1981**, *77*, 2867–2876.
- (39) Yamashita, Y.; Kunieda, H.; Oshimura, E.; Sakamoto, K. Formation of intermediate micellar phase between hexagonal and discontinuous cubic liquid crystals in brine/*N*-acylamino acid surfactant/*N*-acylamino acid oil system. *J. Colloid Interface Sci.* **2007**, *312*, 172–178.
- (40) Wu, J. P.; Zhang, J.; Zheng, L. Q.; Zhao, X. Y.; Li, Na.; Dong, B. Characterization of lyotropic liquid crystalline phases formed in imidazolium based ionic liquids. *Colloids Surf. A* **2009**, *336*, 18–22.
- (41) Gu, Y. Q.; Shi, L. J.; Gao, H. J.; Li, J.; Zheng, L. Q. Phase behavior of didecylpyrrolidinium bromide in aqueous solution. *Colloids Surf. A* **2013**, *420*, 82–88.
- (42) Cordobes, F.; Munoz, J.; Gallegos, C. Linear viscoelasticity of the direct hexagonal liquid crystalline phase for a heptane/nonionic surfactant/water system. *J. Colloid Interface Sci.* **1997**, *187*, 401–417.
- (43) Shi, L. J.; Zhao, M. W.; Zheng, L. Q. Lyotropic liquid crystalline phases formed in ternary mixtures of *N*-alkyl-*N*-methylpyrrolidinium bromide/1-decanol/water. *RSC Adv.* **2012**, *2*, 11922–11929.
- (44) Haas, S.; Hoffmann, H.; Thunig, C.; Hoinkis, E. Phase and aggregation behaviour of double-chain cationic surfactants from the class of *N*-alkyl-*N*-alkyl’-*N,N*-dimethylammonium bromide surfactants. *Colloid Polym. Sci.* **1999**, *277*, 856–867.
- (45) Frisch, M. J.; Trucks, G. W.; Schlegel, H. B.; Scuseria, G. E.; Robb, M. A.; Cheeseman, J. R.; Scalmani, G.; Barone, V.; Mennucci, B.; Petersson, G. A.; Nakatsuji, H.; Caricato, M.; Li, X.; Hratchian, H. P.; Izmaylov, A. F.; Bloino, J.; Zheng, G.; Sonnenberg, J. L.; Hada, M.; Ehara, M.; Toyota, K.; Fukuda, R.; Hasegawa, J.; Ishida, M.; Nakajima, T.; Honda, Y.; Kitao, O.; Nakai, H.; Vreven, T.; Montgomery, J. A., Jr.; Peralta, J. E.; Ogliaro, F.; Bearpark, M.; Heyd, J. J.; Brothers, E.; Kudin, K. N.; Staroverov, V. N.; Keith, T.; Kobayashi, R.; Normand, J.; Raghavachari, K.; Rendell, A.; Burant, J. C.; Iyengar, S. S.; Tomasi, J.; Cossi, M.; Rega, N.; Millam, J. M.; Klene, M.; Knox, J. E.; Cross, J. B.; Bakken, V.; Adamo, C.; Jaramillo, J.; Gomperts, R.; Stratmann, R. E.; Yazyev, O.; Austin, A. J.; Cammi, R.; Pomelli, C.; Ochterski, J. W.; Martin, R. L.; Morokuma, K.; Zakrzewski, V. G.; Voth, G. A.; Salvador, P.; Dannenberg, J. J.; Dapprich, S.; Daniels, A. D.; Farkas, Ö.; Foresman, J. B.; Ortiz, J. V.; Cioslowski, J.; Fox, D. J. *Gaussian 09*, revision A.02; Gaussian, Inc.: Wallingford, CT, 2009.
- (46) Tanford, C. Micelle shape and size. *J. Phys. Chem.* **1972**, *76*, 3020–3024.
- (47) Weimann, M.; Fárník, M.; Suhm, M. A.; Alikhani, M. E.; Sadlej, J. Cooperative and anticooperative mixed mrimers of HCl and methanol. *J. Mol. Struct.* **2006**, *790*, 18–26.
- (48) Das, D.; Dey, J.; Chandra, A. K.; Thapa, U.; Ismail, K. Aggregation behavior of sodium dioctylsulfosuccinate in aqueous ethylene glycol medium. A case of hydrogen bonding between

surfactant and solvent and its manifestation in the surface tension isotherm. *Langmuir* **2012**, *28*, 15762–15769.

(49) Pan, A.; Mati, S. S.; Naskar, B.; Bhattacharya, S. C.; Moulik, S. P. Self-aggregation of MEGA-9 (*N*-nonanoyl-*N*-methyl-D-glucamine) in aqueous medium: Physicochemistry of interfacial and solution behaviors with special reference to formation energetics and micelle microenvironment. *J. Phys. Chem. B* **2013**, *117*, 7578–7592.

(50) Mitchell, D. J.; Ninham, B. W. Micelles, vesicles and microemulsions. *J. Chem. Soc., Faraday Trans. 2* **1981**, *77*, 601–629.

(51) Israelachvili, J. N.; Mitchell, D. J.; Ninham, B. W. Theory of self-assembly of hydrocarbon amphiphiles into micelles and bilayers. *J. Chem. Soc., Faraday Trans. 2* **1976**, *72*, 1525–1568.

(52) Lin, Y. Y.; Qiao, Y.; Yan, Y.; Huang, J. B. Thermo-responsive viscoelastic wormlike micelle to elastic hydrogel transition in dual-component systems. *Soft Matter* **2009**, *5*, 3047–3053.

(53) Wei, X. L.; Ping, A. Li.; Du, P. P.; Liu, J.; Sun, D. Z.; Zhang, Q. F.; Hao, H. G.; Yu, H. J. Formation and properties of wormlike micelles in solutions of a cationic surfactant with a 2-hydroxypropoxy insertion group. *Soft Matter* **2013**, *9*, 8454–8463.

(54) Mishra, B. K.; Samant, S. D.; Pradhan, P.; Mishra, S. B.; Manohar, C. A new strongly flow birefringent surfactant system. *Langmuir* **1993**, *9*, 894–898.

(55) Horbaschek, K.; Hoffmann, H.; Thunig, C. Formation and properties of lamellar phases in systems of cationic surfactants and hydroxy-naphthoate. *J. Colloid Interface Sci.* **1998**, *206*, 439–456.

(56) Hao, J. C.; Hoffmann, H. Self-assembled structures in excess and salt-free catanionic surfactant solutions. *Curr. Opin. Colloid Interface Sci.* **2004**, *9*, 279–293.